Robust Finite-Time Control Tracking Via an Enhancing Supertwisting with Application to UAVs

Moussa Labbadi

Robust Finite-Time Control Tracking Via an Enhancing *Supertwisting* with Application to UAVs

Moussa Labbadi, Member, IEEE

***Abstract*— This study deals with an underactuated unmanned aerial vehicle tracking control problem in finite time under disturbances. The two control loops that make up the hierarchical finite-time controller are the inner-loop rotation control and the outer-loop translation control. It was constructed using a predetermined terminal sliding manifold and a high-order sliding mode control. Using a modified supertwisting method, we offer a unique Lyapunov-based predefined-time control technique for z-position in translation control. For both x and y positions, a simple controller is then used. Roll, pitch, and yaw motions have been subjected to rotation control using high order sliding mode control with a predefined-time sliding mode manifold. Numerical simulation results are presented to illustrate how well the suggested control system works in trajectory tracking and disturbances.**

***Index Terms*— Quadrotors; fixed-time tracking control; matched perturbations.**

I. Introduction

The past few decades have seen a significant increase in the study of unmanned aerial vehicles (UAVs), driven by their unique benefits in carrying out missions in hazardous and inaccessible environments. Typical rotary-wing UAVs with the ability to take off and land vertically are called quadrotors(QR), and they are especially well-suited for a variety of possible uses, including mapping, rescue, surveillance, and transportation [1]. The development of autonomous control algorithms for QR is crucial for the emergence of these applications, which presents a number of difficulties. Initially, the designed controller needs to have good closed-loop performance, quick response times, and resilience to outside shocks and model uncertainty. To guarantee the viability of the achieved control actions, input constraints—which typically stem from the physical restrictions of actuators—should also be taken into account.

A. Related Works

The ability of UAVs to fly precisely and smoothly is one of their most difficult tasks. Some of these include the sliding mode control (SMC) [2], [3], adaptive control [4], neural network [5], backstepping approach [6], etc. Regarding evaluating the effectiveness of completing time-sensitive flight missions, the convergence speed of the formation control system is crucial since the QR UAV cluster cannot precisely complete the task before the intended formation shape has been established [7]. In addition to having the benefit of strong robustness to shocks and high formation efficiency, the finite-time formation control approach can guarantee the closed-loop system's finite-time convergence. A recursive integral terminal sliding function-based adaptive controller was proposed in [8]. In [9], the finite-time stabilization of the QR using the global terminal sliding mode control is suggested. The authors in [12] proposed an adaptive super twisting sliding mode control technique for robust control of the six-DOF nonlinear dynamics of an uncertain air vehicle. An adaptive control strategy based on super-twisting was offered for a UAV with winds in [10], [11]. Obtaining the initial conditions of dynamic systems in practice is also a challenging task [13]. Extending the finite-time stabilization is one method of addressing the problem. One of the advantages of fixed-time stability is the ability to define and modify a uniformly bounded settling-time. Furthermore, the system's states can be stabilized in fixed-time. Specifically when it comes to the formation control of the QR, which needs to quickly converge to the intended formation pattern.

B. Contributions

Based on the above analysis, a generalized supertwisting-based fixed-time sliding mode control (FxT-SMC) is studied for the anti-disturbance tracking control of the quadrotor system. Comparing the suggested technique to other approaches, the numerical simulation demonstrates reduced performance index values and excellent stabilization accuracy. The major contributions of this paper can be summarized in the following points:

- A novel generalized supertwisting algorithm (GSTA) Based-FxTSM control using GSTA scheme. Obtained by combining an improved terminal sliding mode manifold and FxT stability.
- The proposed control approach has been applied to QR systems, and compared to previous works.
- A novel control technique is proposed to address the chattering problem and achieve finite-time convergence for both subsystems.
- Simulation results are also used to confirm the effectiveness of the proposed control for the QR system.

C. Paper organization

The remainders of this study are structured as follows. The system model and control objective of the QR are introduced in Section 2. In Section 3 the design of the proposed controller is given. Section 4 demonstrates the supertwisting manifold and the finite-time QR stability. The results of numerical simulations are shown in Section 5. Finally, Section 6 ends this paper with conclusions.

*.
M. Labbadi is with Aix-Marseille University, LIS UMR CNRS 7020, Marseille, France, moussa.labbadi@lis-lab.fr

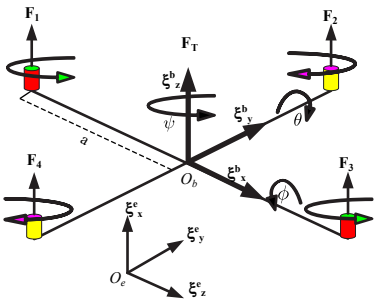

Fig. 1: QR structure design.

II. System modeling

The QR under consideration is a rigid-body aerial vehicle with six degrees of freedom that is maneuvering in three dimensions. A QR typically has four rotors arranged symmetrically and equally spaced from the center, as seen in Fig. 1. F_1, F_2, F_3, and F_4 are the upward-lifting forces produced by the four rotors, which are arranged to spin in two pairs in opposing orientations. Each rotor's spinning speed can be adjusted to provide the force and torque needed to drive the vehicle to carry out specific translation and rotation behaviors.

Two reference frames are established to represent the translational and rotational motions: an earth-fixed inertial frame with origin O_e and axes ξ_x^e, ξ_y^e, and ξ_z^e; the other is a body-fixed frame with O_b and ξ_{bx}^e, ξ_{by}^e, and ξ_{bz}^e. Let define $\mathcal{P} = \begin{bmatrix} x & y & z \end{bmatrix}^T$ as absolute position of the QR which is the coordinate values of the center mass in the fixed frame. The formula for the vehicle's linear velocity with regard to the body-fixed frame is $v = \begin{bmatrix} v_x & v_y & v_z \end{bmatrix}^T$. The QR's attitude, where describes how the body-fixed frame rotates in relation to the earth-fixed frame, is denoted by Euler angles as $\mathcal{Q} = \begin{bmatrix} \phi & \theta & \psi \end{bmatrix}^T$, which the ϕ, θ, ψ are respectively the roll, pitch and yaw angles. Let define the attitude velocity as $\varpi = \begin{bmatrix} \varpi_x & \varpi_y & \varpi_z \end{bmatrix}^T$.

The following differential equation sets depict the dynamic model of the QR around a hovering point that may be built using the Euler-Newton approach.

$$\begin{aligned} &\text{Position system} \begin{cases} \dot{\mathcal{P}} = v \\ m\dot{v} = -m\mathcal{G} + \mathcal{R}(\mathcal{Q})F_T + K_X + \delta_X(t) \end{cases} \\ &\text{Attitude system} \begin{cases} \dot{\mathcal{Q}} = \varpi \\ \mathcal{I}\dot{\varpi} = -\varpi \times \mathcal{I}\varpi + \tau_\varpi + K_\eta + \delta_\Omega(t) \end{cases} \end{aligned} \tag{1}$$

- m is the QR mass;
- $\mathcal{G} = [0\ 0\ -g]^T$ with g being the gravitational acceleration;
- $\mathcal{R}(\mathcal{Q}) = \begin{pmatrix} \sin\theta\cos\psi\cos\phi + \sin\psi\sin\phi \\ \sin\theta\cos\phi\sin\psi - \sin\phi\cos\psi \\ \cos\phi\cos\theta \end{pmatrix}$ is the component of the orthogonal rotation matrix in the direction of e_z^e with $e_z^e = [0\ 0\ 1]^T$;
- $\mathcal{I} = \text{diag}\{J_1, J_2, J_3\}$ is a moments of inertia diagonal matrix;
- $\tau_\varpi = [\tau_x\ \tau_y\ \tau_z]^T$, where τ_i is the quadrotor torque.
- $K_\eta = diag[K_{\eta 1}, K_{\eta 2}, K_{\eta 3}]$ and $K_X = diag[K_x, K_y, K_z]$ are the aerodynamic coefficient matrices. τ_c is the resultant torque due to the gyroscopic effect;
- $\delta_X(t) = diag[\delta_x(t), \delta_y(t), \delta_z(t)]$ and $\delta_\Omega(t) = diag[\delta_{\eta 1}(t), \delta_{\eta 2}(t), \delta_{\eta 3}(t)]$ are the external disturbances.

The QR system's control inputs are the thrust force F_T and the torque vector τ_ϖ. As seen below, they are all produced by the lifting forces F_1, F_2, F_3, and F_4, that the four rotors produce.

$$\begin{bmatrix} F_T \\ \tau_\varpi \end{bmatrix} = \begin{bmatrix} a & a & a & a \\ 0 & -a & 0 & a \\ a & 0 & -a & 0 \\ -a & a & -a & a \end{bmatrix} \begin{bmatrix} F_1 \\ F_2 \\ F_3 \\ F_4 \end{bmatrix} \tag{2}$$

where a is the distance from the rotors to the center of mass of the vehicle.

III. Problem formulation and control strategy

Consider the QR mathematical model, which represents the whole dynamics in the presence of disturbances.

$$\ddot{\phi} = \chi_1\dot{\theta}\dot{\psi} - \chi_2\dot{\theta}\eta - \chi_3\dot{\phi}^2 + \chi_1\tau_x + d_{\eta 1}(t) \tag{3a}$$
$$\ddot{\theta} = \varphi_1\dot{\phi}\dot{\psi} + \varphi_2\dot{\phi}\eta - \varphi_3\dot{\theta}^2 + \varphi_1\tau_y + d_{\eta 2}(t) \tag{3b}$$
$$\ddot{\psi} = \varsigma_1\dot{\phi}\dot{\theta} - \varsigma_2\dot{\psi}^2 + \varsigma_1\tau_z + d_{\eta 3}(t) \tag{3c}$$
$$\ddot{x} = (\sin\theta\cos\psi\cos\phi + \sin\psi\sin\phi)\frac{F_T}{m} - a_x\dot{x} + \delta_x(t) \tag{3d}$$
$$\ddot{y} = (\sin\theta\sin\psi\cos\phi - \sin\phi\cos\psi)\frac{F_T}{m} - a_y\dot{y} + \delta_y(t) \tag{3e}$$
$$\ddot{z} = -g + \cos\theta\cos\phi\frac{F_T}{m} - a_z\dot{z} + \delta_z(t) \tag{3f}$$

$\chi_1 = \frac{J_2 - J_3}{J_1}, \chi_2 = \frac{J_r}{J_1}, \chi_3 = \frac{K_{\eta 1}}{J_1}, \chi_\phi = \frac{1}{J_1}$, $\varphi_1 = \frac{J_3 - J_1}{J_2}, \varphi_2 = \frac{J_r}{J_2}, \varphi_3 = \frac{K_{\eta 2}}{J_2}, \varphi_\theta = \frac{1}{J_2}$, $\varsigma_1 = \frac{J_1 - J_2}{J_3}, \varsigma_2 = \frac{K_{\eta 3}}{J_3}, \varsigma_\theta = \frac{1}{J_3}$, $a_x = \frac{K_x}{m}, a_y = \frac{K_y}{m}, a_z = \frac{K_z}{m}$ where $\omega_q = \omega_1 - \omega_2 + \omega_3 - \omega_4$.

Assumption 1: The Euler angles have the following bounds: θ, $\phi \in [-\frac{\pi}{2}, \frac{\pi}{2}]$ and $\psi \in [-\pi, \pi]$.

Assumption 2: The disturbances $\delta_\eta(t)$ and $\delta_X(t)$ are assumed to be unknown, but their amplitude is limited as $|\delta_X(t)| < \Upsilon_{T1}$ and $|\delta_\eta(t)| < \Upsilon_{T2}$. The time derivative of the disturbances is supposed to be bound such as $\left|\dot{\delta}_X(t)\right| < K_{d1} > 0$ and $\left|\dot{\delta}_\eta(t)\right| < K_{d2} > 0$.

In order to generate the thrust F_T and the desired angles (ϕ_d, θ_d), the virtual controls can be presented as follows:

$$\mathcal{V}_x = (\cos\phi\sin\theta\cos\psi + \sin\phi\sin\psi)\frac{F_T}{m} \tag{4}$$
$$\mathcal{V}_y = (\cos\phi\sin\theta\sin\psi - \sin\phi\cos\psi)\frac{F_T}{m} \tag{5}$$
$$\mathcal{V}_z = -g + (\cos\phi\cos\theta)\frac{F_T}{m} \tag{6}$$

Then, the inverse of (4) are:

$$\phi_d = \arctan\left(\cos\theta_d\frac{\sin\psi_d\mathcal{V}_\mathbf{x} - \cos\psi_d\mathcal{V}_\mathbf{y}}{\mathcal{V}_\mathbf{z} + g}\right) \tag{7a}$$
$$\theta_d = \arctan\left(\frac{\cos\psi_d\mathcal{V}_\mathbf{x} + \sin\psi_d\mathcal{V}_\mathbf{y}}{\mathcal{V}_\mathbf{z} + g}\right) \tag{7b}$$
$$F_T = m\sqrt{\mathcal{V}_\mathbf{x}^2 + \mathcal{V}_\mathbf{y}^2 + (\mathcal{V}_\mathbf{z} + g)^2} \tag{7c}$$

A. Control tracking objective

The control objective is to design a high-order sliding mode control with a FxT convergence of the tracking errors for system. The virtual signal $\mathcal{V}_i = [\mathcal{V}_x,\ \mathcal{V}_y,\ \mathcal{V}_z]^T$ will be designed in order to generate the total thrust F_T and the titling anglers (ϕ_d, θ_d) for the inner loop as shown in Fig. (2), also, the torque controls (τ_x, τ_y, τ_z).

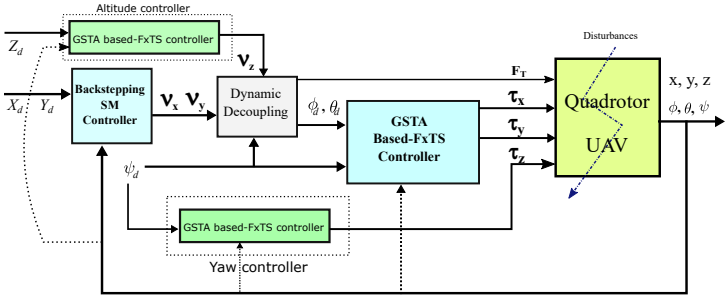

Fig. 2: GSTA based-FxTS Control design.

B. Design tracking control for QR

Let us define the position's tracking errors and their derivatives as follows:

$$\mathbf{e}_x = x - x_d, \quad \mathbf{e}_x = \quad y - y_d, \quad \mathbf{e}_z = z - z_d \tag{8}$$

$$\dot{\mathbf{e}}_x = \dot{x} - \dot{x}_d, \quad \dot{\mathbf{e}}_y = \quad \dot{y} - \dot{y}_d, \quad \dot{\mathbf{e}}_z = \dot{z} - \dot{z}_d \tag{9}$$

Similarly, the tracking errors and its derivatives are defined for the attitude as follows:

$$\mathbf{e}_\phi = \phi - \phi_d, \quad \mathbf{e}_\theta = \quad \theta - \theta_d, \quad \mathbf{e}_\psi = \psi - \psi_d \tag{10}$$

$$\dot{\mathbf{e}}_\phi = \dot{\phi} - \dot{\phi}_d, \quad \dot{\mathbf{e}}_\theta = \quad \dot{\theta} - \dot{\theta}_d, \quad \dot{\mathbf{e}}_\psi = \dot{\psi} - \dot{\psi}_d \tag{11}$$

IV. Controller design

A. Backstepping sliding mode control for Horizontal position

In this part, the horizontal virtual control signals $\mathcal{V}_x$ and $\mathcal{V}_y$ will be designed. These enable to generate the thrust F_T and desired angles $[\phi_d \ \theta_d]^T$. The GSTA-based FxTS controller for the altitude subsystem can ensure rapid convergence to the desired altitude in finite time. However, for position subsystem has three outputs $(z(t), x(t), y(t))$ but it is controlled by only one single control. Hence the fact that the proposed control scheme does not apply to every subsystem. Therefore, to regulate the horizontal position, backstepping with SMC is used.

Let define the sliding mode surface as:

$$\sigma_7(t) = \dot{\mathbf{e}}_x + \Lambda_7 \mathbf{e}_x, \quad \sigma_9(t) = \dot{\mathbf{e}}_x + \Lambda_9 \mathbf{e}_y \tag{12}$$

The time-derivative of these surfaces is,

$$\begin{aligned} \dot{\sigma}_7(t) &= \dot{x}_8(t) - \ddot{x}_d + \Lambda_7 \dot{\mathbf{e}}_x, \\ \dot{\sigma}_9(t) &= \dot{x}_{10}(t) - \ddot{y}_d + \Lambda_{10} \dot{\mathbf{e}}_y \end{aligned} \tag{13}$$

The horizontal position can be controlled by the following laws:

$$\begin{aligned} \mathcal{V}_a =& -\kappa_9 x_8(t) + \ddot{x}_d - \mathbf{e}_x - \kappa_{1x}(\mathbf{e}_x - \kappa_{1x}\mathbf{e}_x) - \kappa_{2x}\text{sign}(\sigma_7(t)) \\ \mathcal{V}_b =& -\kappa_{10} x_{10}(t) + \ddot{y}_d - \mathbf{e}_y - \kappa_{1y}(\mathbf{e}_y - \kappa_{1y}\mathbf{e}_y) - \kappa_{2y}\text{sign}(\sigma_9(t)) \end{aligned} \tag{14}$$

where $\kappa_{1x}, \kappa_{2x}, \kappa_{1y}, \kappa_{2y} > 0$.

B. GSTA based-FxTS Control design for altitude subsystem

In this section, the GSTA based-FxTS altitude subsystem control design, will be presented. In order to achieve fixed-time convergence for both $z(t)$ and $\dot{z}(t)$, we define the following terminal sliding mode variable.

$$\sigma_{11}(t) = \dot{\mathbf{e}}_z + \left\lceil \left\lceil \dot{\mathbf{e}}_z \right\rceil^2 + \mathcal{C}_p \mathbf{e}_z + \mathcal{C}_q \left\lceil \mathbf{e}_z \right\rceil^3 \right\rceil^{\frac{1}{2}}, \tag{15}$$

with,

- $\lceil \mathcal{X} \rceil^* = |\mathcal{X}|^* sign(\mathcal{X})$;
- $\mathcal{C}_p$, and $\mathcal{C}_q$ are positive parameters.

$$\begin{aligned} \dot{\sigma}_{11}(t) &= \ddot{\mathbf{e}}_z + \frac{|\dot{\mathbf{e}}_z|\ddot{\mathbf{e}}_z + \frac{\mathcal{C}_p + \mathcal{C}_q \mathbf{e}_z^3}{2}\dot{\mathbf{e}}_z}{\underbrace{\left|\left\lceil \dot{\mathbf{e}}_z \right\rceil^2 + \mathcal{C}_p \mathbf{e}_z + \mathcal{C}_q \left\lceil \mathbf{e}_z \right\rceil^3\right|^{\frac{1}{2}}}_{\Xi_z(\mathbf{e}_z, \dot{\mathbf{e}}_z)}}, \\ &= \frac{\ddot{\mathbf{e}}_z \Xi_z(\mathbf{e}_z, \dot{\mathbf{e}}_z) + |\dot{\mathbf{e}}_z|\ddot{\mathbf{e}}_z + \frac{\mathcal{C}_p + \mathcal{C}_q \mathbf{e}_z^3}{2}\dot{\mathbf{e}}_z}{\Xi_z(\mathbf{e}_z, \dot{\mathbf{e}}_z)}, \\ &= \frac{\ddot{\mathbf{e}}_z \left(\Xi_z(\mathbf{e}_z, \dot{\mathbf{e}}_z) + |\dot{\mathbf{e}}_z|\right) + \frac{\mathcal{C}_p + \mathcal{C}_q \mathbf{e}_z^3}{2}\dot{\mathbf{e}}_z}{\Xi_z(\mathbf{e}_z, \dot{\mathbf{e}}_z)}, \\ &= \ddot{\mathbf{e}}_z \underbrace{\frac{\left(\Xi_z(\mathbf{e}_z, \dot{\mathbf{e}}_z) + |\dot{\mathbf{e}}_z|\right)}{\Xi_z(\mathbf{e}_z, \dot{\mathbf{e}}_z)}}_{\mathcal{B}_z\left(\Xi_z(\mathbf{e}_z, \dot{\mathbf{e}})\right)} + \underbrace{\frac{\frac{\mathcal{C}_p + \mathcal{C}_q \mathbf{e}_z^3}{2}\dot{\mathbf{e}}_z}{\Xi_z(\mathbf{e}_z, \dot{\mathbf{e}}_z)}}_{\mathcal{A}_z\left(\Xi_z(\mathbf{e}_z, \dot{\mathbf{e}}_z)\right)}, \\ &= \ddot{\mathbf{e}}_z \mathcal{B}_z\left(\Xi_z(\mathbf{e}_z, \dot{\mathbf{e}}_z)\right) + \mathcal{A}_z\left(\Xi_z(\mathbf{e}_z, \dot{\mathbf{e}}_z)\right) \end{aligned} \tag{16}$$

In the following parts of the paper, we use $\mathcal{A}_z$ for $\mathcal{A}_z\left(\Xi_z(\mathbf{e}_z, \dot{\mathbf{e}}_z)\right)$ and $\mathcal{B}_z$ for $\mathcal{B}_z\left(\Xi_z(\mathbf{e}_z, \dot{\mathbf{e}}_z)\right)$. The double time-derivative of the altitude tracking error can be defined as :

$$\ddot{\mathbf{e}}_z = \mathcal{V}_z - a_z \dot{z} + \delta_z(t) - \ddot{z}_d. \tag{17}$$

substituting (17) into (16), we have

$$\dot{\sigma}_{11}(t) = \mathcal{B}_z \mathcal{V}_z - \left(a_z \dot{z} - \delta_z(t) + \ddot{z}_d\right)\mathcal{B}_z + \mathcal{A}_z \tag{18}$$

The equivalent control law is done by setting $\dot{\sigma}_{11}(t) = 0$ without disturbances, then it may be given by :

$$\mathcal{V}_{eqz} = \frac{\left(a_z \dot{z} + \ddot{z}_d\right)\mathcal{B}_z - \mathcal{A}_z}{\mathcal{B}_z}. \tag{19}$$

It is demonstrated in the Theorem 2 on the paper [13] that the system (15) is globally fixed-time stable and with a setting time $\mathcal{T}_z(\mathbf{e}_z(0)) \leq \mathcal{T}_{maxz} = \frac{4\sqrt{2}}{\sqrt{\mathcal{C}_p}} + \frac{4\sqrt{2}}{\sqrt{\mathcal{C}_q}}$. Now, we use a *generalized supertwisting algorithm* [15] to address the chattering problem unlike in the classical *supertwisting algorithm* with a finite-time stability of the sliding variable. The main idea is to use a power fraction on the discontinuity term in STA. In the following part of the paper, the design steps of the GSTA are presented.

$$\begin{aligned} \mathcal{V}_{sz} &= -\left(\eta_z \mathcal{B}_z \left\lceil \sigma_{11}(t) \right\rceil^{\alpha_z} + u_z(t)\right) \\ u_z(t) &= \eta_{\dot{z}} \mathcal{B}_z \left\lceil \sigma_{11}(t) \right\rceil^{\alpha_{\dot{z}}} \end{aligned} \tag{20}$$

where $\alpha_z \in ([1/2], 1)$ and $\alpha_{\dot{z}} = 2\alpha_z - 1$ are positive constants.

Substituting controller (20) into system (3f) obtains

$$\begin{aligned} \dot{\sigma}_z &= \sigma_{\dot{z}} - \eta_z \left\lceil \sigma_{11}(t) \right\rceil^{\alpha_{\dot{z}}} \\ \dot{\sigma}_{\dot{z}} &= -\eta_{\dot{z}} \left\lceil \sigma_{11}(t) \right\rceil^{\alpha_{\dot{z}}} + \dot{\delta}_z(t) \end{aligned} \tag{21}$$

where $\sigma_z = \sigma_{11}(t)$ and $\sigma_{\dot{z}} = \delta_\eta(t) z(t) - \eta_{\dot{z}} \int_0^1 \left\lceil \sigma_{11}(t) \right\rceil^{\alpha_{\dot{z}}} d\tau$.

Remark 4.1: the standard STA contains a discontinuous function $sign(\sigma_z)$, but the provided GSTA (21) does not have any discontinuous terms.

Remark 4.2: It is important to note that the suggested GSTA degenerates into the traditional STA when $\alpha_z = 0.5$. As can be seen, the Lyapunov function for the typical STA is built as $V(\sigma) = \epsilon^T P \epsilon$ where $\epsilon^T = (\epsilon_z, \epsilon_{\dot{z}})$ and P is a asymmetric positive matrix. After that we can ensure the finite-time stability of the system using STA. For our proposed GSTA the Lyapunov function is inapplicable.

So, in the following part, the main results can be found using the proposed control method. A brand-new Lyapunov method will then be developed to confirm it.

Theorem 1: The variables σ_z and $\sigma_{\dot{z}}$ will converge in finite time to the region shown in the following diagram when the SM dynamics (21) with Assumption 1 is taken into account:

$$\text{Region} = \left| \begin{matrix} (\sigma_z, \sigma_{\dot{z}}) : |\sigma_z| \leq t_{\sigma_z} \\ |\sigma_{\dot{z}}| \leq t_{\sigma_{\dot{z}}} \end{matrix} \right| \tag{22}$$

with $t_{\sigma_z} = \lambda_{\dot{z}}^{\frac{1}{2-\alpha_z+\alpha_{\dot{z}}}} \left(\frac{\lambda_z K_{d1}}{\lambda_z(1-p)}\right)^{\frac{1}{\alpha_{\dot{z}}}} \left[\left(\frac{2}{\alpha_z}\right) + 2^{0.5}\right]$ and $t_{\sigma_{\dot{z}}} = \eta_z^{\frac{1}{2-\alpha_z+\alpha_{\dot{z}}}} \left(\frac{2}{\alpha_z}\right)^{\frac{\alpha_z}{2}} \left(\frac{\lambda_z K_{d1}}{\lambda_z(1-p)}\right)^{\frac{\alpha_z}{\alpha_{\dot{z}}}}$.
λ_z and $\lambda_{\dot{z}}$ are positive constants, and $p \in (0,1)$ is an arbitrarily small parameter.

Proof: Define new variables as: $z_z = \sigma_z$ and $z_{\dot{z}} = \frac{1}{\eta_z}\sigma_{\dot{z}}$, the system (21) becomes

$$\begin{aligned} \dot{z}_z &= \rho_z(z_{\dot{z}} - \lceil z_z \rceil^{\alpha_z} \\ \dot{z}_{\dot{z}} &= -\rho_{\dot{z}} \lceil z_z \rceil^{\alpha_{\dot{z}}} + \frac{\dot{\delta}_z(t)}{\rho_z} \end{aligned} \tag{23}$$

with $\rho_z = \eta_z$ and $\rho_z = \frac{\eta_{\dot{z}}}{\eta_z}$. Next step, we define a new system as

$$\begin{aligned} \dot{z}_z &= \rho_z \varrho_z \\ \dot{z}_{\dot{z}} &= \rho_{\dot{z}}(\varrho_{\dot{z}} + \varrho_3) + \frac{\dot{\delta}_z(t)}{\rho_z} \end{aligned} \tag{24}$$

with $\varrho_z = -\lceil z_z \rceil^{\alpha_z} + z_{\dot{z}}$, $\varrho_3 = -\lceil z_{\dot{z}} \rceil^{\frac{\alpha_{\dot{z}}}{\alpha_z}}$, $\varrho_3 = \lceil z_{\dot{z}} \rceil^{\frac{\alpha_{\dot{z}}}{\alpha_z}} + \lceil z_z \rceil^{\alpha_{\dot{z}}}$ and $\varrho_4 = -z_z + \lceil z_{\dot{z}} \rceil^{\frac{1}{\alpha_z}}$.

Stimulated by the work in [15], [16], the Lyapunov function can be selected as

$$V(z_z, z_{\dot{z}}) = \Upsilon_z + \Upsilon_{\dot{z}}, \tag{25}$$

with $\Upsilon_z = 0.5(z_z - \lceil z_{\dot{z}} \rceil^{\frac{1}{\alpha_z}})^2$ $\Upsilon_{\dot{z}} = 0.5\alpha_z |z_{\dot{z}}|^{\frac{2}{\alpha_z}}$. We can follow the same steps in [15] to demonstrate the finite-time convergence. ∎

C. GSTA based-FxTS inner-loop control design

In this section, the GSTA based-FxTS attitude subsystems control design, will be presented. To achieve fixed-time convergence for both $\phi(t), \theta(t), \psi(t), \dot{\phi}(t), \dot{\theta}(t)$ and $\dot{\psi}(t)$, we define the following terminal sliding mode variables.

$$\sigma_\phi(t) = \dot{\mathbf{e}}_\phi + \left\lceil \left\lceil \dot{\mathbf{e}}_\phi \right\rceil^2 + \mathcal{C}p_\phi \mathbf{e}_\phi + \mathcal{C}q_\phi \left\lceil \mathbf{e}_\phi \right\rceil^3 \right\rceil^{\frac{1}{2}} \tag{26}$$

$$\sigma_\theta(t) = \dot{\mathbf{e}}_\theta + \left\lceil \left\lceil \dot{\mathbf{e}}_\theta \right\rceil^2 + \mathcal{C}p_\theta \mathbf{e}_\theta + \mathcal{C}q_\theta \left\lceil \mathbf{e}_\theta \right\rceil^3 \right\rceil^{\frac{1}{2}} \tag{27}$$

$$\sigma_\psi(t) = \dot{\mathbf{e}}_\psi + \left\lceil \left\lceil \dot{\mathbf{e}}_\psi \right\rceil^2 + \mathcal{C}p_\psi \mathbf{e}_\psi + \mathcal{C}q_\psi \left\lceil \mathbf{e}_\psi \right\rceil^3 \right\rceil^{\frac{1}{2}} \tag{28}$$

with, $\mathcal{C}_{p_{\phi,\theta,\psi}}$, and $\mathcal{C}_{q_{\phi,\theta,\psi}}$ are positive parameters.

Therefore, the time-derivative of these surfaces is as follows:

$$\begin{aligned} \dot{\sigma}_\phi(t) &= \ddot{\mathbf{e}}_\phi + \underbrace{\frac{|\dot{\mathbf{e}}_\phi| \ddot{\mathbf{e}}_\phi + \frac{\mathcal{C}_{p_\phi} + \mathcal{C}_{q_\phi} \mathbf{e}_\phi^3}{2} \dot{\mathbf{e}}_\phi}{\left| \left\lceil \dot{\mathbf{e}}_\phi \right\rceil^2 + \mathcal{C}_{p_\phi} \mathbf{e}_\phi + \mathcal{C}_{q_\phi} \left\lceil \mathbf{e}_\phi \right\rceil^3 \right|^{\frac{1}{2}}}}_{\Xi_\phi(\mathbf{e}_\phi, \dot{\mathbf{e}}_\phi)}, \\ &= \frac{\ddot{\mathbf{e}}_\phi \Xi_\phi(\mathbf{e}_\phi, \dot{\mathbf{e}}_\phi) + |\dot{\mathbf{e}}_\phi| \ddot{\mathbf{e}}_\phi + \frac{\mathcal{C}_{p_\phi} + \mathcal{C}_{q_\phi} \mathbf{e}_\phi^3}{2} \dot{\mathbf{e}}_\phi}{\Xi_\phi(\mathbf{e}_\phi, \dot{\mathbf{e}}_\phi)}, \\ &= \frac{\ddot{\mathbf{e}}_\phi \left(\Xi_\phi(\mathbf{e}_\phi, \dot{\mathbf{e}}_\phi) + |\dot{\mathbf{e}}_\phi|\right) + \frac{\mathcal{C}_{p_\phi} + \mathcal{C}_{q_\phi} \mathbf{e}_\phi^3}{2} \dot{\mathbf{e}}_\phi}{\Xi_\phi(\mathbf{e}_\phi, \dot{\mathbf{e}}_\phi)}, \\ &= \ddot{\mathbf{e}}_\phi \underbrace{\frac{\left(\Xi_\phi(\mathbf{e}_\phi, \dot{\mathbf{e}}_\phi) + |\dot{\mathbf{e}}_\phi|\right)}{\Xi_\phi(\mathbf{e}_\phi, \dot{\mathbf{e}}_\phi)}}_{\mathcal{B}_\phi\left(\Xi_\phi(\mathbf{e}_\phi, \dot{\mathbf{e}})\right)} + \underbrace{\frac{\frac{\mathcal{C}_{p_\phi} + \mathcal{C}_{q_\phi} \mathbf{e}_\phi^3}{2} \dot{\mathbf{e}}_\phi}{\Xi_\phi(\mathbf{e}_\phi, \dot{\mathbf{e}}_\phi)}}_{\mathcal{A}_\phi\left(\Xi_\phi(\mathbf{e}_\phi, \dot{\mathbf{e}}_\phi)\right)}, \\ &= \ddot{\mathbf{e}}_\phi \mathcal{B}_\phi \left(\Xi_\phi(\mathbf{e}_\phi, \dot{\mathbf{e}}_\phi)\right) + \mathcal{A}_\phi \left(\Xi_\phi(\mathbf{e}_\phi, \dot{\mathbf{e}}_\phi)\right) \end{aligned} \tag{29}$$

Besides, using the same calculations, we find the sliding manifold of attitude subsystems

$$\dot{\sigma}_\phi(t) = \ddot{\mathbf{e}}_\phi \mathcal{B}_\phi \left(\Xi_\phi(\mathbf{e}_\phi, \dot{\mathbf{e}}_\phi)\right) + \mathcal{A}_\phi \left(\Xi_\phi(\mathbf{e}_\phi, \dot{\mathbf{e}}_\phi)\right) \tag{30}$$

$$\dot{\sigma}_\theta(t) = \ddot{\mathbf{e}}_\theta \mathcal{B}_\theta \left(\Xi_\theta(\mathbf{e}_\theta, \dot{\mathbf{e}}_\theta)\right) + \mathcal{A}_\theta \left(\Xi_\theta(\mathbf{e}_\theta, \dot{\mathbf{e}}_\theta)\right) \tag{31}$$

$$\dot{\sigma}_\psi(t) = \ddot{\mathbf{e}}_\psi \mathcal{B}_\psi \left(\Xi_\psi(\mathbf{e}_\psi, \dot{\mathbf{e}}_\psi)\right) + \mathcal{A}_\psi \left(\Xi_\psi(\mathbf{e}_\psi, \dot{\mathbf{e}}_\psi)\right) \tag{32}$$

In the following parts of the paper, we use $\mathcal{A}_\zeta$ for $\mathcal{A}_\Phi\left(\Xi_\zeta(\mathbf{e}_\zeta, \dot{\mathbf{e}}_\zeta)\right)$ and $\mathcal{B}_\zeta$ for $\mathcal{B}_\zeta\left(\Xi_\zeta(\mathbf{e}_\zeta, \dot{\mathbf{e}}_\zeta)\right)$ with $\zeta = \{\phi, \theta, \psi\}$.

The double time-derivative of the altitude tracking error can be defined as :

$$\ddot{\mathbf{e}}_\zeta = \mathcal{V}_\zeta - a_\zeta \dot{\zeta} + \delta_\zeta(t) - \ddot{\zeta}_d. \tag{33}$$

substituting (33) into (29), we have

$$\dot{\sigma}_\zeta(t) = \mathcal{B}_\zeta \mathcal{V}_\zeta - \left(a_\zeta \dot{\zeta} - \delta_\zeta(t) + \ddot{\zeta}_d\right)\mathcal{B}_\zeta + \mathcal{A}_\zeta \tag{34}$$

The equivalent control law is done by setting $\dot{\sigma}_\zeta(t) = 0$ without disturbances, then it may be given by :

$$\begin{aligned} \mathcal{V}_{\phi_{eq}} &= \frac{\left(a_\phi \dot{\phi} + \ddot{\phi}_d\right)\mathcal{B}_\phi - \mathcal{A}_\phi}{\mathcal{B}_\phi}. \\ \mathcal{V}_{\theta_{eq}} &= \frac{\left(a_\theta \dot{\theta} + \ddot{\theta}_d\right)\mathcal{B}_\theta - \mathcal{A}_\theta}{\mathcal{B}_\theta}. \\ \mathcal{V}_{\psi_{eq}} &= \frac{\left(a_\psi \dot{\psi} + \ddot{\psi}_d\right)\mathcal{B}_\psi - \mathcal{A}_\psi}{\mathcal{B}_\psi}. \end{aligned} \tag{35}$$

In the following part of the paper, the design steps of the GSTA of the attitude subsystem are presented.

$$\begin{aligned} \mathcal{V}_{s_\zeta} &= -\left(c_{\zeta 1} \lceil \sigma_\zeta(t) \rceil^{\alpha_\zeta} + u_\zeta(t)\right) \\ u_\zeta(t) &= \quad c_{\zeta 2} \lceil \sigma_\zeta(t) \rceil^{\alpha_{\dot{\zeta}}} \end{aligned} \tag{36}$$

where $\alpha_\zeta \in ([1/2], 1)$, $\zeta 1, \zeta 2$ and $\alpha_{\dot{\zeta}} = 2\alpha_\zeta - 1$ are positive constants.

Substituting controller (36) into attitude subsystem obtains

$$\begin{aligned} \dot{\sigma}_\zeta &= \sigma_{\dot{\zeta}} - c_{\zeta 1} \lceil \sigma_\zeta(t) \rceil^{\alpha_\zeta} \\ \dot{\sigma}_{\dot{\zeta}} &= -c_{\zeta 2} \lceil \sigma_\zeta(t) \rceil^{\alpha_{\dot{\zeta}}} + \dot{\delta}_\zeta(t) \end{aligned} \tag{37}$$

where $\sigma_\zeta = \sigma_\zeta(t)$ and $\sigma_{\dot{\zeta}} = \delta_\eta(t)\zeta(t) - \eta_{\dot{\zeta}} \int_0^1 \lceil \sigma_\zeta(t) \rceil^{\alpha_{\dot{\zeta}}} d\tau$.

Theorem 2: The variables σ_ζ and $\sigma_{\dot{\zeta}}$ will finite-time converge to the region shown in the following diagram when the SM dynamics (37) with Assumption 1 is taken into account:

$$\text{Region} = \left| \begin{matrix} (\sigma_\zeta, \sigma_{\dot{\zeta}}) : |\sigma_\zeta| \leq t_{\sigma_\zeta} \\ |\sigma_{\dot{\zeta}}| \leq t_{\sigma_{\dot{\zeta}}} \end{matrix} \right| \tag{38}$$

with $t_{\sigma_\zeta} = \lambda_{\dot{\zeta}}^{\frac{1}{2-\alpha_\zeta+\alpha_{\dot{\zeta}}}} \left(\frac{\lambda_\zeta K_{d2}}{\lambda_\zeta(1-p)}\right)^{\frac{1}{\alpha_{\dot{\zeta}}}} \left[\left(\frac{2}{\alpha_\zeta}\right) + 2^{0.5}\right]$ and $t_{\sigma_{\dot{\zeta}}} = \eta_\zeta^{\frac{1}{2-\alpha_\zeta+\alpha_{\dot{\zeta}}}} \left(\frac{2}{\alpha_\zeta}\right)^{\frac{\alpha_\zeta}{2}} \left(\frac{\lambda_\zeta K_{d2}}{\lambda_\zeta(1-p)}\right)^{\frac{\alpha_\zeta}{\alpha_{\dot{\zeta}}}}$.
λ_ζ and $\lambda_{\dot{\zeta}}$ are positive constants, and $p_\zeta \in (0,1)$ is an arbitrarily small parameter.

Proof: Define new variables as: $V_\zeta = \sigma_\zeta$ and $V_{\dot{\zeta}} = \frac{1}{\eta_\zeta}\sigma_{\dot{\zeta}}$, the system (21) becomes

$$\begin{aligned} \dot{V}_\zeta &= \rho_\zeta(V_{\dot{\zeta}} - sig(V_\zeta, \alpha_\zeta)) \\ \dot{V}_{\dot{\zeta}} &= -\rho_{\dot{\zeta}} sig(V_\zeta, \alpha_{\dot{\zeta}}) + \frac{\dot{\delta}_\zeta(t)}{\rho_\zeta} \end{aligned} \tag{39}$$

with $\rho_\zeta = \eta_\zeta$ and $\rho_{\dot{\zeta}} = \frac{\eta_{\dot{\zeta}}}{\eta_\zeta}$. Next step, we define a new system as

$$\begin{aligned} \dot{V}_\zeta &= \rho_\zeta \varrho_\zeta \\ \dot{V}_{\dot{\zeta}} &= \rho_{\dot{\zeta}}(\varrho_{\dot{\zeta}} + \varrho_3) + \frac{\dot{\delta}_\zeta(t)}{\rho_\zeta} \end{aligned} \tag{40}$$

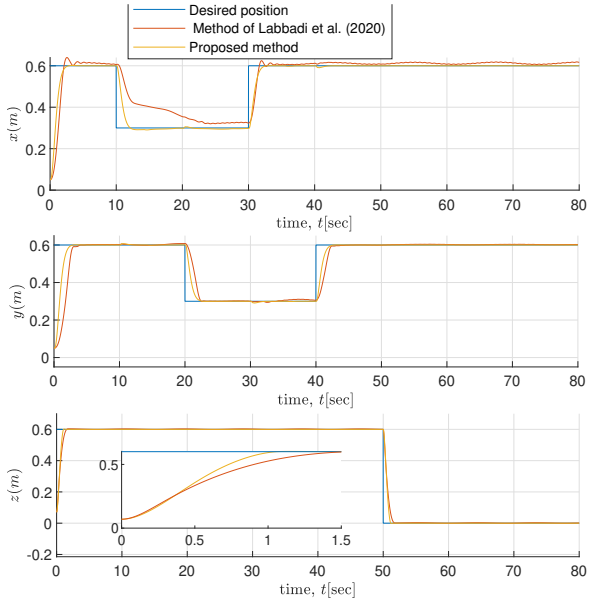

Fig. 3: Position trajectory tracking.

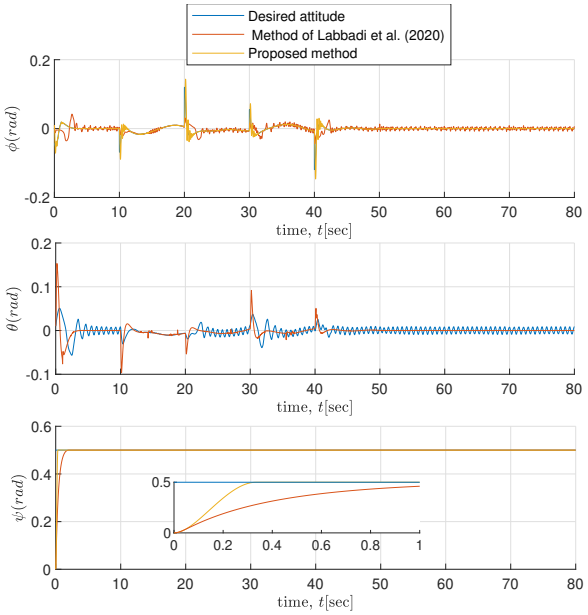

Fig. 4: Attitude trajectory tracking.

with $\varrho_\zeta = -sig(V_\zeta, \alpha_\zeta) + V_{\dot{\zeta}}$, $\varrho_3 = -sig(V_{\dot{\zeta}}, \frac{\alpha_{\dot{\zeta}}}{\alpha_\zeta})$, $\varrho_3 = sig(V_{\dot{\zeta}}, \frac{\alpha_{\dot{\zeta}}}{\alpha_\zeta}) + sig(V_\zeta, \alpha_{\dot{\zeta}})$ and $\varrho_4 = -V_\zeta + sig(V_{\dot{\zeta}}, \frac{1}{\alpha_\zeta})$.

Stimulated by the work in [15], [16], the Lyapunov function can be selected as

$$V(V_\zeta, V_{\dot{\zeta}}) = \Upsilon_\zeta + \Upsilon_{\dot{\zeta}}, \tag{41}$$

with $\Upsilon_\zeta = 0.5(V_\zeta - sig(V_{\dot{\zeta}}, \frac{1}{\alpha_\zeta})^2$ $\Upsilon_{\dot{\zeta}} = 0.5\alpha_\zeta |V_{\dot{\zeta}}|^{\frac{2}{\alpha_\zeta}}$. We can follow the same steps in [15] to demonstrate the finite-time convergence. ■

V. Simulation Study Results

In this section, we present simulation tests in term tracking trajectories in the presence of complex perturbations. The proposed control is tested with a complex trajectory. In order to validate its performance, a finite-time controller is used for a comparison. This later was developed in [17] as operate on all results by "Method of Labbadi et al. (2020)". The QR parameters in the simulations are illustrated in the Table I. In the simulations, the following disturbances are used.

$$\begin{aligned}
\delta_x(t) &= (.8\sin(\pi(t-30)/31) + 0.4\sin(\pi(t-30)/7) \\
&\quad + .08\sin(\pi(t-30)/2) + .056\sin(\pi(t-30)/11)), \\
&\quad m/s^2], \quad t \in [10, 30]; \quad \delta_x(t) = 0, \quad m/s^2], \quad \text{else} \\
\delta_y(t) &= 0.5\sin(0.4t) + 7.5\cos(0.7t), m/s^2], \quad t \in [10, 50] \\
&\quad \delta_y(t) = 0, \quad m/s^2, \quad \text{else} \\
\delta_y(t) &= 0.5\cos(0.7t) + 0.7\sin(0.3t), m/s^2] \\
\delta_\phi(t) &= 0.5\cos(0.4t) + 1, \quad rad/s^2, \\
\delta_\theta(t) &= 0.5\sin(0.5t) + 1, \quad rad/s^2, \\
\delta_\psi(t) &= .5\sin(0.7t) + 1, \quad rad/s^2, \quad t \in [0, 10]
\end{aligned}$$

The results of the tracking performance of the proposed control and method developed in [17] are depicted in Figs. 3-7. The linear position is plotted in Fig. 3. It is clear these results demonstrate the finite-time convergence of the errors and position states. However, the results provided by the [17] present high oscillations on the states with some in the start time on all states. This demonstrate our proposed controller is better than the Ref. [17]. The finite-time convergence of the attitude is shown in Fig. 4. Fig. 5 displays the time evolution of the control signals for position and attitude. Also, the results in 3D and 2D demonstrate the finite-time convergence of the proposed control method as show in Figs. 6 and 7.

TABLE I: QR parameters.

Parameter	Value	Parameter	Value
$g(m/s^2)$	9.8	$k_{dy}(Nms^2)$	0.01
$m(kg)$	2	$k_{dz}(Nms^2)$	0.01
$I_{11}(kg.m^2)$	0.016	$k_{ax}(Nrads^2)$	0.012
$I_{22}(kg.m^2)$	0.016	$k_{ay}(Nrads^2)$	0.012
$I_{33}(kg.m^2)$	0.032	$k_{az}(Nrads^2)$	0.012
$J_r(kg.m^2)$	2.8385e-5	$b_k(N.s^2)$	2.9842e-3
$k_{dx}(Nms^2)$	0.01	$c_d(N.m.s^2)$	3.2320e-2

VI. Conclusions

A dual-loop, finite-time hierarchical control scheme for QR exposed to complicated disturbances is presented in this study. To construct the outer-loop translation controller and the inner-loop rotational controller, a high-order sliding mode control-based supertwisting framework is integrated with a predefined-time sliding mode manifold. Using a preset surface as a basis, the high faster property of the inner-loop rotation controller is designed and precisely characterized using fixed-time stability theory. Next, in order to handle the discontinuous term on the traditional supertwisting algorithm, we applied a generalized supertwisting algorithm. The z-position control has been subjected to the rotational controller step. Extensive simulation analyses confirm that the suggested hierarchical control architecture is effective.

References

[1] Mofid, O.; Mobayen, S.; Mobayen, S.; Mobayen, S.; Zhang, C.; Esakki, B. Desired Tracking of Delayed Quadrotor UAV Under Model Uncertainty and Wind Disturbance Using Adaptive Super-twisting Terminal Sliding Mode Control. 2021, doi:10.1016/J.ISATRA.2021.06.002.

[2] Zheng, E.-H.; Xiong, J.-J.; Luo, J.-L. Second Order Sliding Mode Control for a Quadrotor UAV. 2014, 53, doi:10.1016/J.ISATRA.2014.03.010.

[3] Benaddy, A.; Labbadi, M.; Elyaalaoui, K.; Bouzi, M. Fixed-Time Fractional-Order Sliding Mode Control for UAVs under External Disturbances. Fractal Fract. 2023, 7, 775. https://doi.org/10.3390/fractalfract7110775

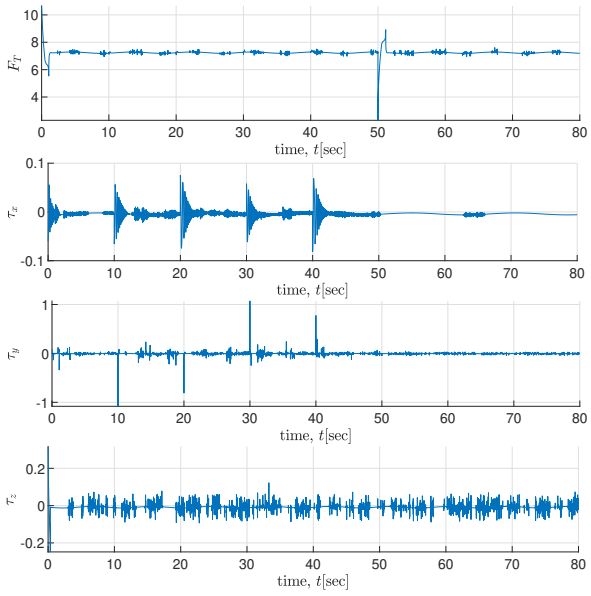

Fig. 5: Input control signals.

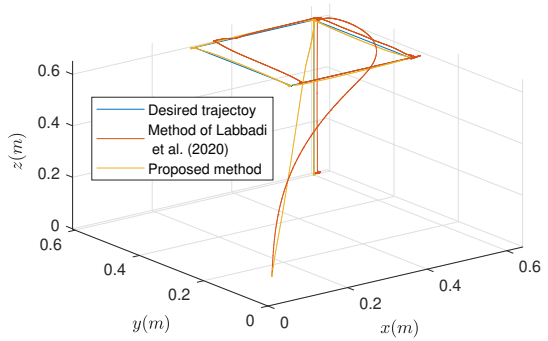

Fig. 6: 3D trajectory tracking.

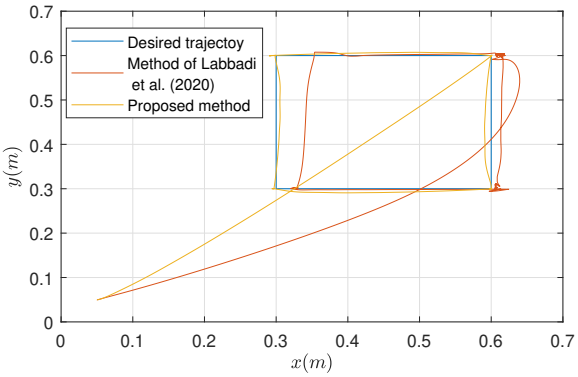

Fig. 7: 2D trajectory tracking.

[4] Mofid, O.; Mobayen, S. Adaptive Sliding Mode Control for Finite-time Stability of Quad-rotor Uavs with Parametric Uncertainties. 2017, 72, doi:10.1016/J.ISATRA.2017.11.010.

[5] Zhao, Z.-Y.; Jin, X.-Z.; Wu, X.-M.; Wang, H.; Chi, J. Neural Network-based Fixed-time Sliding Mode Control for a Class of Nonlinear Euler-lagrange Systems. 2022, 415, doi:10.1016/J.AMC.2021.126718.

[6] Jiang, T.; Lin, D.; Song, T. Finite-time Backstepping Control for Quadrotors with Disturbances and Input Constraints. 2018, 6, doi:10.1109/ACCESS.2018.2876558.

[7] Mechali, O.; Xu, L.; Xie, X.; Iqbal, J. Theory and Practice for Autonomous Formation Flight of Quadrotors via Distributed Robust Sliding Mode Control Protocol with Fixed-time Stability Guarantee. 2022, 123, doi:10.1016/j.conengprac.2022.105150.

[8] Shao, K.; Zheng, J.; Huang, K.; Wang, H.; Man, Z.; Fu, M. Finite-time Control of a Linear Motor Positioner Using Adaptive Recursive Terminal Sliding Mode. 2020, 67, doi:10.1109/TIE.2019.2937062.

[9] Xiong, J.-J.; Zhang, G.-B. Global Fast Dynamic Terminal Sliding Mode Control for a Quadrotor UAV. 2017, 66, doi:10.1016/J.ISATRA.2016.09.019.

[10] Cui, L.; Zhang, R.; Yang, H.; Zuo, Z. Adaptive Super-twisting Trajectory Tracking Control for an Unmanned Aerial Vehicle Under Gust Winds. 2021, 115, doi:10.1016/J.AST.2021.106833.

[11] Nassiri, S.; Labbadi, M.; Cherkaoui, M. Optimal Integral Super-twisting Sliding-mode Control for High Efficiency of Pumping Systems. IEEE Control Systems Letters, 2022, 55, doi:10.1016/j.ifacol.2022.07.317.

[12] Babaei, A.-R.; Malekzadeh, M.; Madhkhan, D. Adaptive Super-twisting Sliding Mode Control of 6-DOF Nonlinear and Uncertain Air Vehicle. 2019, 84, doi:10.1016/J.AST.2018.09.013.

[13] Polyakov, A. Nonlinear Feedback Design for Fixed-time Stabilization of Linear Control Systems. IEEE Transactions on Automatic Control, vol. 57, no. 8, pp. 2106-2110, Aug. 2012, doi:10.1109/TAC.2011.2179869.

[14] Labbadi, M.; Cherkaoui, M. Adaptive Fractional-order Nonsingular Fast Terminal Sliding Mode Based Robust Tracking Control of Quadrotor UAV with Gaussian Random Disturbances and Uncertainties. 2021, 57, 2265–2277, doi:10.1109/TAES.2021.3053109.

[15] Mei, Keqi, Shihong Ding, and Xinghuo Yu. A generalized super-twisting algorithm. IEEE Transactions on Cybernetics (2022).

[16] H. Du, C. Qian, S. Yang, and S. Li, Recursive design of finite-time convergent observers for a class of time-varying nonlinear systems, Automatica, vol. 49, no. 2, pp. 601–609, Feb. 2013.

[17] M. Labbadi and M. Cherkaoui , Robust adaptive nonsingular fast terminal sliding-mode tracking control for an uncertain quadrotor UAV subjected to disturbances. ISA Transactions . Elsevier, 2020, vol.99, p.290–304. DOI: 10.1016/j.isatra.2019.10.012.